Available online at www.sciencedirect.com
SCIENCE DIRECT
Journal of volcanology and geothermal research
ELSEVIER
Journal of Volcanology and Geothermal Research 149 (2006) 139–159
www.elsevier.com/locate/jvolgeores

Magma mixing during the 2001 event at Mount Etna (Italy): Effects on the eruptive dynamics

M. Viccaro [a], C. Ferlito [a], L. Cortesogno [b], R. Cristofolini [a,*], L. Gaggero [b]

[a] *Dipartimento di Scienze Geologiche, Università di Catania, Corso Italia 55, I-95129 Catania, Italy*
[b] *Dipartimento per lo Studio del Territorio e delle sue Risorse, Università di Genova, Corso Europa 26, I-16132 Genova, Italy*

Received 5 November 2004; received in revised form 18 May 2005; accepted 19 June 2005

Abstract

During the 2001 eruptive episode three different magmas were erupted on the southern flank of Mount Etna volcano from distinct vent systems. Major and minor element chemistry of rocks and minerals shows that mixing occurred, and that the mixed magma was erupted during the last eruptive phases.

The space–time integrated analysis of the eruption, supported by geophysical data, together with major and trace element bulk chemistry (XRF, ICP-MS) and major and trace mineral chemistry (EPMA, LAM ICP-MS), support the following model: 1) trachybasaltic magma rises through a NNW–SSE trending structure, connected to the main open conduit system; 2) ascent of an amphibole-bearing trachybasaltic magma from a 6 km deep eccentric reservoir through newly open N–S trending fractures; 3) just a few days following the eruption onset the two tectonic systems intersect at the Laghetto area; 4) at the Laghetto vent a mixed magma is erupted.

Mixing occurred between the amphibole-bearing trachybasaltic magma and an inferred deep more basic end-member. The most relevant aspect in the eruptive dynamics is that the eruption of the mixed magma at the Laghetto vent was highly explosive due to volatile content in the magma. The gas phase formed, mainly because of the decreased volatile solubility due to rapid fractures opening and increased *T*, related to mixing, and partially because of the amphibole breakdown.

Keywords: Mount Etna; summit-parasitic eruptions; magma mixing; gas exsolution; eruptive dynamics

1. Introduction

Mount Etna (3340 m a.s.l.) is a composite volcano (cf. Romano, 1982) along to the Ionian coast-line of eastern Sicily, Italy. Its activity started with eruptions of tholeiitic lavas in the late-Pleistocene and evolved into Na-alkaline products, having consistently increased in the last 200 ka (Gillot et al., 1994; Romano, 1982). Lately, in particular during the last few centuries, the Etnean activity has consisted in summit and flank eruptions, prevailingly effusive, with strombolian ejections, producing almost exclusively lapilli and

* Corresponding author. Tel.: +39 095 7195752; fax: +39 095 7195760.
E-mail address: rcristof@unict.it (R. Cristofolini).

0377-0273/$ - see front matter © 2005 Elsevier B.V. All rights reserved.
doi:10.1016/j.jvolgeores.2005.06.004

scoriae. Most of the flank eruptions of the past century have occurred along regionally controlled fracture systems, the NE–SW one on the north-eastern flank, and the NNW–SSE trending lineaments on the southern and south-eastern flank; here activity has been particularly intense over the last two decades, concentrated at the recently formed (1971) South-East summit vent and at many parasitic vents, with significantly increased frequency of eruptive episodes and rates (Lo Giudice and Rasà, 1986; Acocella and Neri, 2003).

At first the 2001 eruption took place mainly in the higher southern sector of Mt. Etna with vents in the summit area at the South-East crater and south of the Montagnola, down to 2100 m a.s.l., and later at the Piano del Lago (Fig. 1). The eruption was preceded by a large earthquake swarm a few days before its onset and associated to relevant ground deformation and fracture opening. The development of ground cracks along with the hypocentral distribution pattern allowed two distinct eruptive systems, simultaneously active to be defined, trending NNW–SSE and N–S respectively,

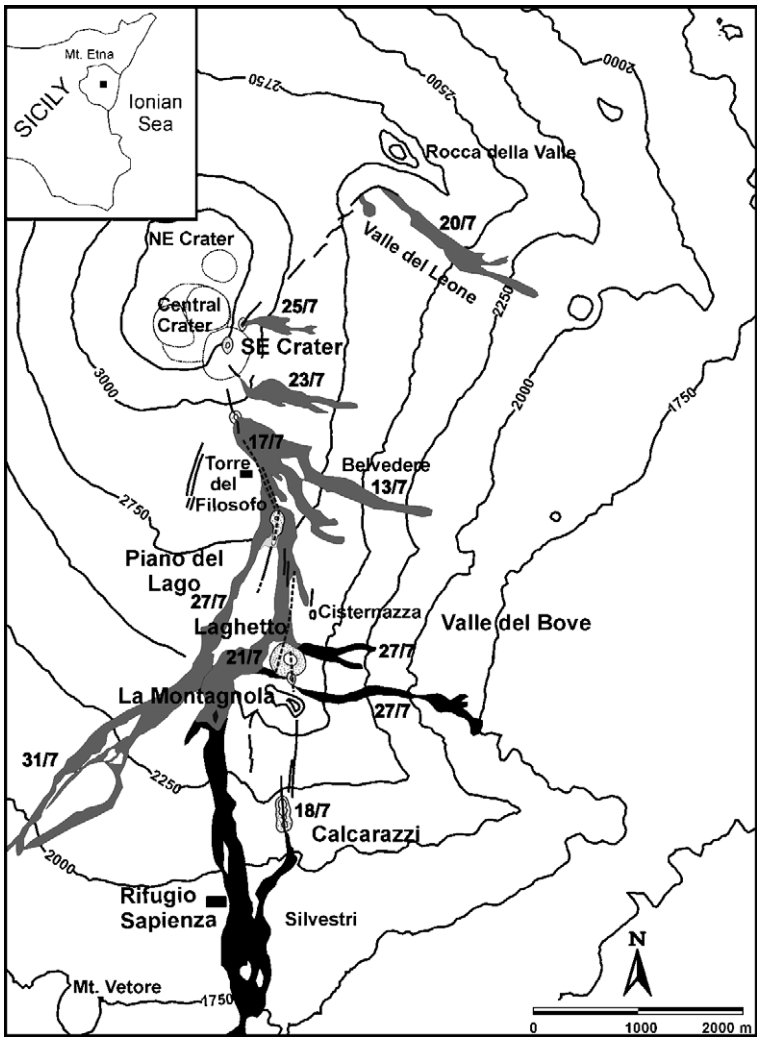

Fig. 1. Sketch map of SE–PL and C–L fracture systems, vents and lava flows of 2001 eruptive event. Solid lines represent visible fissures; dashed lines represent fissures buried by lava flows. SE–PL lavas are light grey; EC–L and LC–L lavas are in black. All dates refer to the onset of the relative lava flow.

along with a third minor one directed NE–SW (Monaco et al., 2005). Erupted lavas are mainly trachybasalts, with petrological and distinct compositional characteristics, with reference to their vent sites and times of eruption. The eruption produced on the whole an estimated volume of about 25×10^6 m^3 of lava and 7×10^6 m^3 (DRE) of tephra (Behncke and Neri, 2003; Clocchiatti et al., 2004; Lautze et al., 2004). High explosivity, fracture fields with various trends, and two distinct compositions of the erupted magma led several authors to consider the 2001 eruption as among the most relevant of the last few years. On the grounds of a detailed and temporally controlled sampling of lavas and tephra, this paper points out that a relationship exists among fracture systems, vent setting and magma compositions, and gives evidence for the hypothesis that one of the two magmas could have partially mixed with a third one, not erupted as such, and finally relates the observed changes of the eruptive behaviour to the distinct magmas progressively involved in the eruption.

2. Time evolution of the July–August 2001 eruptive episode

The seismic and volcanological events have been described in detail in reports by the INGV-Sezione di Catania staff (www.ct.ingv.it) and in Behncke and Neri (2003); only information strictly related to the eruptive period is reported here in a summarized way and integrated by personal field observations.

The eruption occurred between July 13th and August 9th 2001 on the upper slopes of Mt. Etna (Fig. 1). The first eruptive episode, lava fountaining at the South-East crater (July 13th), was preceded by a cluster of shallow earthquakes located with their foci distributed between 1.5 km a.s.l and 2.0 km b.s.l., below the South-East crater area (Alparone et al., 2004). The opening of fractures on the southern slope of the volcano, between 2800 and 2000 m a.s.l., eruptive at first at their lower end, was heralded by a long-lasting seismic swarm, starting on July 12th, with epicentres distributed along a NNW–SSE oriented plane, at depths between 1.5 km a.s.l. and 4 km b.s.l. (Privitera et al., 2001; Bonaccorso et al., 2002; Patanè et al., 2002; Billi et al., 2003; Lanzafame et al., 2003). The hypocentre distribution vs. time showed a decreasing number of deeper events in the first two days. Later on, from July 15th to 18th earthquakes were concentrated only within the first 2 km below the surface (Monaco et al., 2005).

On the basis of field observations, the fractures on the southern flank of the volcano have been grouped into two systems: an upper one, from the South-East crater (3000 m a.s.l.) to Piano del Lago, named SE–PL, and a lower one, from Calcarazzi (2100 m a.s.l.) to the Laghetto area (2550 m a.s.l.), named C–L.

2.1. The South-East crater–Piano del Lago (SE–PL) system

The eruption started at the South-East crater on July 13th, with lava fountaining related to a little lava flow. On July 13th and 14th, fractures developed from north to south in the area of Piano del Lago forming a NNW–SSE trending anastomized network that reached the western margin of Valle del Bove (Fig. 1). On July 17th an eruptive fissure, directed NNW–SSE, which opened at the southern base of the South-East crater, between 3040 and 2940 m a.s.l., with strombolian and effusive activity that resulted in the formation of three aligned spatter spires and a southerly directed lava flow. Ground fracturing propagated downslope between 2900 and 2800 m a.s.l. and formed a N160–170° trending graben. The lowermost end of this structure propagated in a N15–20° direction, and reached the Piano del Lago crack field at about 2750 m a.s.l. Along this 600 m long fissure, two groups of driblet cones developed at about 2780 and 2720 m a.s.l., while a well fed lava flow poured out and expanded in a south-westerly direction down to 2000 m a.s.l.

The night between July 19th and 20th, activity resumed at the South-East crater; a new set of NE–SW trending fissures opened and the lowermost end of this new fracture system shifted sharply eastwards, where the fractures met the high relief of Rocca della Valle. Lava was emitted from this elbow, at an elevation of 2680 m a.s.l., into the Valle del Leone, with a low output rate (<2 m^3/s; Behncke and Neri, 2003). Finally, on July 23rd, a 100 m long NNW–SSE fracture opened on the southern flank of the South-East crater, and a small lava flow came out directed eastwards to the Valle del Bove.

2.2. The Calcarazzi–Laghetto (C–L) system

During the night between July 17th and 18th, N–S oriented ground fractures opened south of the Montagnola and west of Mt. Calcarazzi at about 2100 m a.s.l.. Lava flows were emitted from the lowest portion of these fractures, and advanced southward (Fig. 1). Lava crossed the main road to Nicolosi, and flowed east of the Rifugio Sapienza, reaching its lowest elevation (1035 m a.s.l.) seven days later.

In the meanwhile ground fracturing extended northwards from the Calcarazzi area with an overall length of about 1 km up to 2550 m a.s.l., at the Laghetto area (north of the Montagnola). Here the fractures met and intersected the SE–PL ones that were extending southward. On July 21st, a pit crater opened there and ejected mostly ash-laden steam and abundant lithic tephra with spectacularly high thrust columns (about 300 m above the edge of the pit crater) and a convective plume, related to phreatomagmatic explosive activity and conduit widening (Coltelli et al., 2001; Taddeucci et al., 2002, 2004; Behncke and Neri, 2003). Starting on July 24th, ash and steam emissions evolved to a markedly magmatic lava fountaining up to 500 m high. During a two-week period a 120 m high cinder cone was formed through explosive activity. Between July 26th and 31st lava flowed from the southern base of the new cone down to about 2000 m a.s.l., and destroyed the upper cable-car station and pillars (Calvari and Pinkerton, 2004).

3. Sampling and analytical methods

The various flow units were sampled in detail, taking into account their succession in time and the setting of their eruptive vents. A total of 26 rock samples were collected; 9 samples from the base of the South-East crater and the Belvedere lava flow, related to the SE–PL system; 17 samples from lavas emitted by the C–L system, subdivided into: 5 samples, close to the lowermost front of the lava flow, representing the earlier lavas (EC–L), and 12 samples collected just before the end of the eruption at the 2100 m vent and at the Laghetto cone, representing the late emitted products of the C–L system (LC–L).

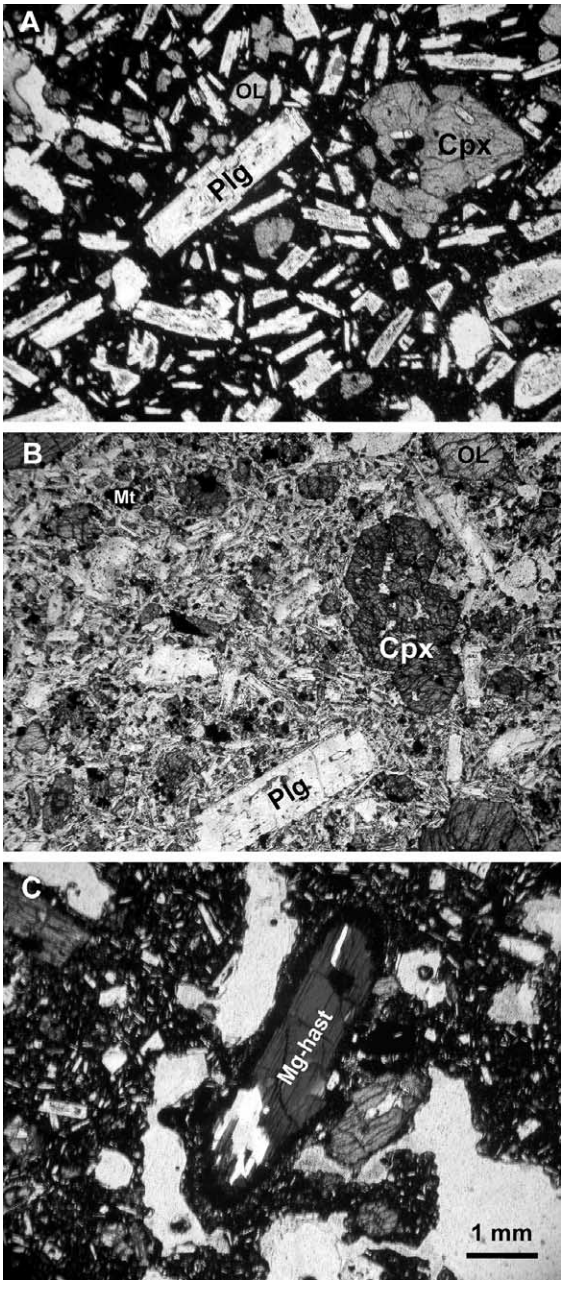

Fig. 2. A) Abundant tabular plagioclase phenocrysts (up to 0.5 cm) in a cryptocrystalline groundmass in SE–PL lava; phenocrysts of clinopyroxene are subordinate and olivine is scarce. B) Clinopyroxene and subordinate plagioclase, olivine and Ti-magnetite phenocrysts are present in EC–L lava; the holocrystalline groundmass is mainly composed of plagioclase microphenocrysts. C) Megacryst of Mg-hastingsite in EC–L lava; a characteristic semi-opaque rim is clearly evident. All photos are taken with parallel Nicols and have the same scale bar.

Major element whole rock compositions were analysed by XRF on powder pellets, corrected for matrix effects (Franzini et al., 1972), at the Dipartimento di Scienze Geologiche, University of Catania; loss on ignition (L.O.I.) was determined by gravimetric method. RE and minor element abundances were analysed by ICP-MS at the SGS Laboratories, Canada.

Major elements in the mineral phases were analysed by means of a Philips SEM 515 scanning electron microscope (Dip.Te.Ris., University of Genoa) equipped with an EDAX PV9100 spectrometer in the energy dispersive mode, at 15 kV accelerating voltage and 2.1 mA beam current.

Plagioclase cation values were normalized to 8 oxygens and pyroxene atomic proportions were calculated assuming stoichiometry and charge balance (Wood and Banno, 1973). Pyroxene nomenclature follows the scheme of Morimoto et al. (1988), extended by Rock (1990) to Na–Ca and Na–pyroxenes. The Ca-amphibole was named after Leake et al. (1997), and its A.U.F. was normalized to 13 − (Ca + Na + K); Fe^{3+} was computed in order to obtain a cation charge = 46, and $Fe^{2+} = Fe_{tot} - Fe^{3+}$; $Al^{IV} = 8 - Si$, $Al^{VI} = Al_{tot} - Al^{IV}$.

Minor and trace elements for plagioclase, clinopyroxene and amphibole were analyzed too by laser ablation microprobe inductively coupled plasma mass spectrometry (LAM ICP MS) at CNR-Dipartimento di Geoscienze e Georisorse, Pavia. The basic setup of the instrument is described in Bottazzi et al. (1999), with the most important modification consisting in the adoption of a shorter laser wavelength (213 nm) resulting from mixing of the fundamental radia-

Table 1
Selected major element concentrations in plagioclase phenocrysts at core, rim and middle spot (int) of EC–L, LC–L and SE–PL lavas

Sample	10.2A3	10.2A4	10.2A5	15.2A6	15.2A2	33.2A1	33.2A2	35.2A2	35.2A3
Location	EC–L	EC–L	EC–L	LC–L	LC–L	LC–L	LC–L	SE–PL	SE–PL
Position	CORE	INT	RIM	CORE	RIM	CORE	INT	CORE	RIM
SiO_2	46.39	46.60	48.19	52.52	54.43	53.50	52.82	49.65	54.73
TiO_2	0.14	0.13	0.10	0.13	0.22	0.19	0.21	0.15	0.19
Cr_2O_3	0.13	0.16	0.18	0.18	0.05	0.24	0.27	0.21	0.18
Al_2O_3	32.9	32.79	31.92	28.17	27.89	27.97	28.91	30.66	27.36
Fe_2O_3	0.36	/	/	0.56	/	/	/	0.62	0.86
FeO	0.27	0.69	0.59	0.25	0.75	0.8	0.77	0.27	/
MnO	/	/	0.03	0.06	0.07	0.08	0.10	0.01	0.05
MgO	/	/	/	/	0.14	/	/	/	/
NiO	/	/	0.01	0.04	/	0.13	0.30	0.08	/
CaO	17.86	17.79	16.69	12.89	12.09	12.47	13.63	15.57	11.36
Na_2O	1.30	1.01	1.71	3.97	3.63	4.06	3.45	2.57	5.16
K_2O	0.21	0.22	0.30	0.53	0.72	0.64	0.62	0.40	0.63
Total	99.56	99.39	99.72	99.30	99.99	100.10	101.10	100.20	100.50
Si	2.152	2.171	2.228	2.412	2.49	2.439	2.394	2.278	2.467
Ti	0.005	0.005	0.004	0.005	0.008	0.007	0.007	0.005	0.006
Cr	0.005	0.006	0.007	0.007	0.002	0.009	0.01	0.008	0.006
Al	1.799	1.8	1.739	1.525	1.503	1.503	1.544	1.658	1.453
Fe^{3+}	0.013	/	/	0.019	/	/	/	0.021	0.029
Fe^{2+}	0.01	0.027	0.023	0.01	0.029	0.031	0.029	0.01	/
Mn	/	/	0.001	0.002	0.003	0.003	0.004	/	0.002
Mg	/	/	/	/	0.01	/	/	/	/
Ni	/	/	/	0.002	/	0.005	0.011	0.003	/
Ca	0.888	0.888	0.827	0.634	0.593	0.609	0.662	0.765	0.549
Na	0.117	0.091	0.153	0.354	0.322	0.359	0.303	0.229	0.451
K	0.012	0.013	0.018	0.031	0.042	0.037	0.036	0.023	0.036
Anorthite	87	90	83	62	62	61	66	75	53
Albite	12	9	15	35	34	36	30	23	44
Orthoclase	1	1	2	3	4	3	4	2	3

tion (1064 nm) and the fourth harmonic radiation (266 nm) into a third harmonic generator (Jeffries et al., 1998).

4. Characteristics of the erupted rocks

4.1. Petrography and mineral chemistry

The SE–PL and C–L lavas show markedly distinct textures and modal compositions.

4.1.1. SE–PL

SE–PL lavas are porphyritic (P.I. 30–40) with a seriate texture; their phenocrysts occur in a generally hypocrystalline groundmass (Fig. 2A) and are strongly zoned plagioclase, augitic-clinopyroxene, and olivine in volume ratios around 64%, 31% and 5% respectively; Ti-magnetite and apatite are found as accessory phases. The textural relations among the phenocrysts suggest an early crystallization of Ti-magnetite, olivine and plagioclase followed by clinopyroxene.

Plagioclase phenocrysts are strongly zoned (An_{80} cores and An_{52} rims) with low Or (2–4 mol%) (Table 1). FeO_{tot} content is notable (0.61–0.93 wt.%), similar to that of other Etnean plagioclases, and higher at phenocryst cores, probably related to glassy microinclusions (sieve-texture).

The RE and other minor element analysis of two plagioclase grains was carried out at their rims and cores. The normalized REE patterns (Anders and Ebihara, 1982) are very homogeneous, showing LREE enrichment ($\Sigma LREE = 22$; $La_N/Sm_N = 16$) and marked HREE fractionation ($Sm_N/Yb_N = 10$) with $Eu/Eu^* = 14$ (Fig. 3; Table 2).

The spider diagram (Anders and Ebihara, 1982) shows high Ba_N, La_N, Sr_N, Ti_N and Sc_N values, with positive spikes for Eu_N, and negative ones for Nb_N, Zr_N and Gd_N (Fig. 4).

Clinopyroxene compositions fall in the augite field at the boundary with diopside, typically representative of alkali basalt pyroxenes, with a wide range of Al_2O_3 (3.9–6.9 wt.%) and SiO_2 (47–50 wt.%) and Al slightly in excess of $Si + Al = 2$ (Table 3).

The Chondrite normalized REE patterns (Anders and Ebihara, 1982) of 4 spot analyses come out as highly homogeneous, with La less enriched than Sm

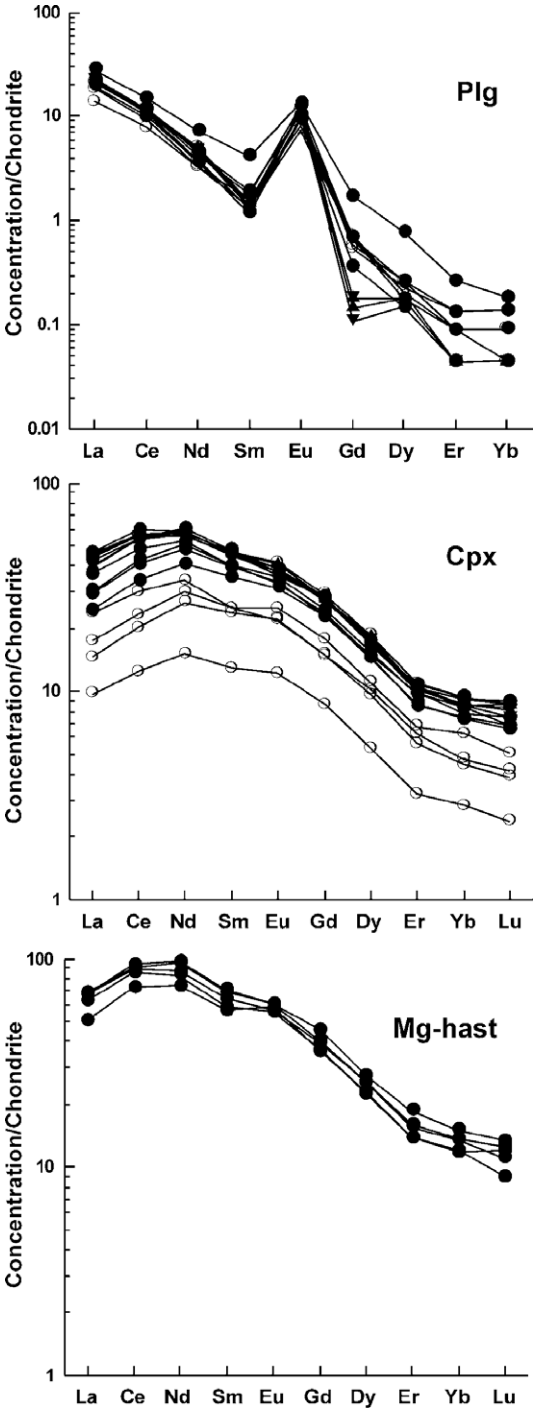

Fig. 3. Chondrite normalized (Anders and Ebihara, 1982) REE patterns for plagioclase, clinopyroxene and Mg-hastingsite phenocrysts in C–L (filled circles: cores; empty circles: rims) and SE–PL lavas (filled up-triangles: cores; filled down-triangles: rims).

Table 2
Selected trace element concentrations in plagioclase phenocrysts at core, rim and middle spot (int) of EC–L, LC–L and SE–PL lavas

Sample	10.2A3	10.2A4	10.2A5	15.2A6	15.2A2	33.2A1	33.2A2	35.2A2	35.2A3
Location	EC–L	EC–L	EC–L	LC–L	LC–L	LC–L	LC–L	SE–PL	SE–PL
Position	CORE	INT	RIM	CORE	RIM	CORE	INT	CORE	RIM
Li	/	<0.39	<0.47	/	2	4	2	/	/
Sc	2	3	2	2	4	4	4	1	1
V	1	1	1	1	3	5	8	2	2
Cr	2	<0.60	<0.74	/	3	<0.62	4	<1.52	/
Co	0.1	0.2	0.2	0.3	0.3	0.9	1.2	0.24	0.23
Sr	2182	2730	2711	1934	1830	2625	2154	1471	1494
Y	0.21	0.23	0.21	0.21	0.21	0.31	0.88	0.11	0.1
Zr	0.2	0.1	0.2	0.5	0.4	/	/	/	/
Nb	0.03	0.2	0.2	0.01	0.3	0.2	0.2	0.3	0.3
Ba	130	92	117	211	309	324	306	240	2342
La	7.2	4.6	6.2	6.5	7.1	6.9	9.3	7.7	7.6
Ce	10.3	6.8	8.3	8.7	9.3	9.9	13.1	10.2	10.1
Pr	0.85	0.62	0.74	0.76	0.85	0.87	1.24	0.86	0.85
Nd	2.89	2.09	2.11	2.3	3.2	2.7	4.6	3.2	3.1
Sm	0.39	0.27	0.33	0.24	0.3	0.36	0.85	0.3	0.28
Eu	0.8	0.57	0.63	0.73	0.88	0.98	1.03	0.91	0.89
Gd	0.19	0.19	0.2	0.1	0.15	0.19	0.48	0.05	0.05
Tb	0.02	0.02	0.02	0.01	0.03	0.02	0.05	0.01	0.01
Dy	0.06	0.07	0.07	0.05	0.08	0.09	0.27	0.06	0.06
Ho	0.01	0.02	0.02	0.01	0.02	0.02	0.04	0.02	0.01
Er	0.02	0.02	0.01	0.01	0.03	0.03	0.06	0.01	0.01
Yb	0.02	0.01	0.01	0.01	<0.0204	0.03	0.04	0.01	0.01
Lu	/	<0.0020	<0.0032	/	/	<0.0033	0.01	0.01	0.01
Hf	0.02	<0.0088	0.01	0.02	0.03	<0.0133	0.15	0.04	0.04
Ta	/	<0.0031	0.01	0.01	0.02	0.05	0.09	0.02	0.02
Pb	1.41	0.77	0.95	0.95	1.4	1.1	1.7	0.66	0.66
Th	0.01	/	0.02	0.01	0.04	0.11	0.33	<0.0014	/
U	/	<0.0007	/	0.01	0.02	0.06	0.11	<0.0048	/

and a strong HREE fractionation ($Sm_N/Yb_N=5.28$). (Fig. 3; Table 4).

In the spider diagram (Anders and Ebihara, 1982), the patterns are highly homogeneous with low values of Ba_N, Nb_N, Cr_N, Sr_N, Zr_N and Ti_N whereas Sc_N exhibits a positive anomaly (Fig. 4).

Olivine is $Fo_{76–70}$, with scarce tephroite and monticellite components. Fo values are consistent with the range found by Clocchiatti et al. (2004) for olivine in the 2001 lavas erupted from high elevation vents.

Ti-magnetite composition is about Mt 48 mol% and Usp 52 mol%. TiO_2 and MgO contents are 13 wt.% and 4.7 wt.% respectively, with Al_2O_3 up to 6 wt.%.

4.1.2. C–L

In C–L lavas P.I. ranges between 10 and 20, with a mesophyric seriate texture; phenocrysts are augitic clinopyroxene (40–50 vol.%), plagioclase (35–45 vol.%), olivine (~5 vol.%), Ti-magnetite (~3 vol.%) and Ca-amphibole (up to 6 vol.%) (Fig. 2B–C). The amphibole is megacrystic (up 10 cm long) and poikilitic, mainly enclosing plagioclase and clinopyroxene. Amphibole crystals are characteristically rimmed by a semi-opaque envelope (~0.2 mm thick at maximum), due to dehydration related to eruptive decompression (cf. Clocchiatti and Tanguy, 2001). According to Clocchiatti et al. (2004) these rims are made of a mixture of fassäte, rhönite and anorthite with an interstitial K-rich residual glass. Based on textural features Ti-magnetite, olivine and plagioclase are the first crystallized phases followed by clinopyroxene and finally amphibole. Sieve-textures are frequently found at plagioclase phenocryst cores. The holocrystalline groundmass is made up of clinopyroxene, pla-

gioclase and olivine with Ti-magnetite and apatite as accessory phases; the total absence of amphibole microlites must be noted.

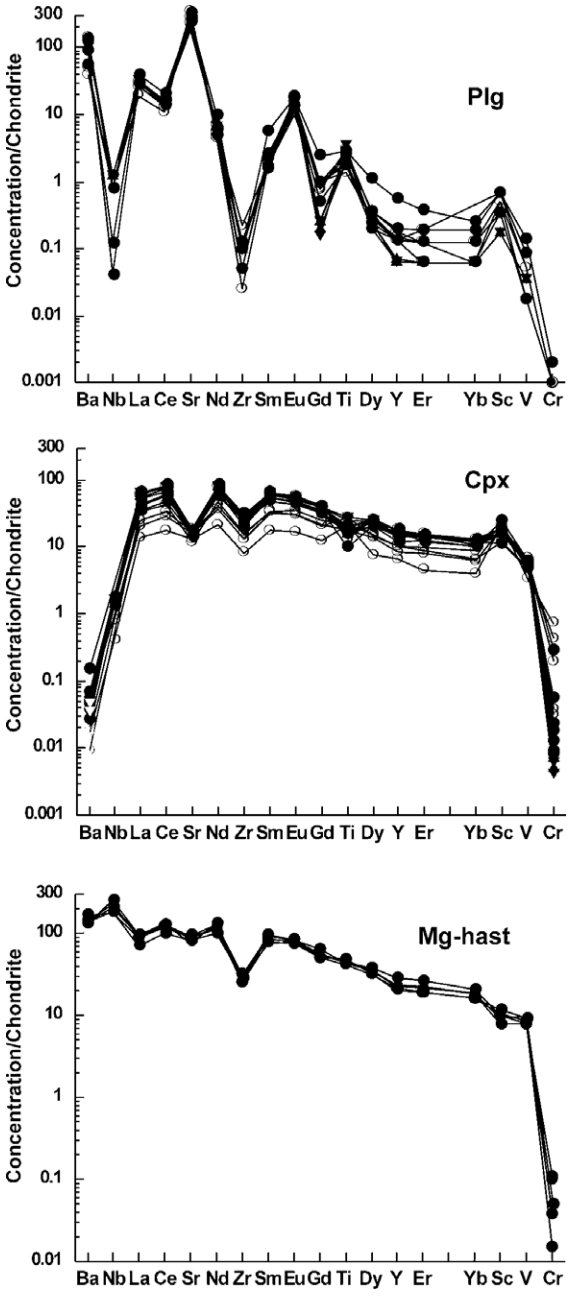

Fig. 4. Chondrite normalized (Anders and Ebihara, 1982) multi-elements (incompatible and compatible) patterns for plagioclase, clinopyroxene and Mg-hastingsite phenocrysts in C–L and SE–PL lavas. For symbols see Fig. 3.

Plagioclase phenocrysts are relatively homogeneous (~An_{90}), even when sieve-textures are developed (Table 1). A thin Na-enriched rim (An_{60}) is very often present and the average composition of groundmass plagioclase is An_{74}. Its FeO_{tot} content is relatively high (0.54–1.1 wt.%).

RE and other minor element compositions have been analyzed at cores and rims of 4 plagioclase grains. The Chondrite normalized REE patterns (Anders and Ebihara, 1982) of cores are homogeneous, with the exception of one sample, and like those of plagioclase cores in SE–PL rocks. LREE abundances are higher at the cores ($\Sigma LREE$=19–29) than at the rims ($\Sigma LREE$=14–21), whereas core and rim HREE concentrations are similar (0.9–1.9 and 0.8–1.1 respectively; Fig. 3; Table 2). Nb_N and Zr_N values are lower in C–L than in SE–PL plagioclase (Fig. 4).

Clinopyroxene is augite at the boundary with diopside. Crystals are weakly zoned, with the highest Mg#=78; major elements distribution is comparable with that of SE–PL clinopyroxenes (SiO_2=45–51 wt.%; Al_2O_3=2.7–9.4 wt.%; Table 3).

The Chondrite normalized REE patterns (Anders and Ebihara, 1982) for 12 spot analyses show homogeneous core compositions similar to those of SE–PL (Fig. 3). At the rims a marked depletion of all REE, Zr, and Y is observed (Fig. 4; Table 4); finally, Cr contents are significantly higher (up to 2000 ppm) than in the cores. These differences are not observed in SE–PL pyroxene.

Amphibole is Mg-hastingsite (Leake et al., 1997; Fig. 2C), differing from the kaersutite amphibole of older Etnean volcanics (Klerkx, 1968; Cristofolini and Lo Giudice, 1969; Cristofolini and Romano, 1982; Cristofolini et al., 1981, 1988); comparison of the 2001 Mg-hastingsite with these kaersutites revealed that the former has lower Na and slightly higher K contents; furthermore, its TiO_2 contents are lower (~3 wt.%; Table 5), which might be related to a late crystallization of Mg-hastingsite, preceded by Ti-magnetite.

The Chondrite normalized patterns (Anders and Ebihara, 1982) show REE fractionation (La_N/Yb_N=4–5), relatively low La (17–23 ppm) and slightly positive Eu anomaly (Eu/Eu^*=1.06–1.26) (Fig. 3; Table 6).

The spider diagram (Anders and Ebihara, 1982) shows LILE slightly fractionated vs. HFSE, enriched

Table 3
Selected major element concentrations in clinopyroxene phenocrysts at core and rim of EC–L, LC–L and SE–PL lavas

Sample	5.2A1	5.2A4	10.2A1	10.2A3	33.2A1	33.2A2	34.2A1	34.2A2	35.2A1	35.2A3
Location	EC–L	EC–L	EC–L	EC–L	LC–L	LC–L	LC–L	LC–L	SE–PL	SE–PL
Position	CORE	RIM	CORE	RIM	CORE	RIM	CORE	CORE	CORE	RIM
SiO_2	49.55	46.33	48.87	51.25	47.23	47.22	48.03	51.06	48.52	47.43
TiO_2	1.18	1.98	1.17	0.95	1.17	1.25	1.19	0.72	1.39	1.77
Al_2O_3	4.46	7.47	5.35	2.69	6.70	7.66	5.93	3.17	5.18	6.78
Fe_2O_3	2.18	4.53	3.36	2.51	4.64	3.39	3.73	0.91	2.74	4.52
FeO	5.82	4.46	4.71	6.00	6.36	4.01	4.59	6.05	5.75	3.70
MnO	0.19	0.18	0.17	0.30	0.38	0.14	0.20	0.16	0.22	0.25
MgO	14.28	12.21	13.56	14.44	10.78	13.17	13.61	15.08	13.18	12.96
CaO	22.21	22.27	22.34	22.04	22.92	22.98	21.98	21.93	22.23	22.88
Na_2O	/	0.36	0.28	0.23	0.25	/	0.10	/	0.23	0.18
K_2O	0.13	0.19	0.17	0.21	0.20	0.17	0.26	0.17	0.08	0.20
Total	100.00	99.98	99.98	100.62	100.63	99.99	99.62	99.25	99.52	100.67
Si	1.840	1.732	1.813	1.890	1.764	1.751	1.790	1.900	1.816	1.749
Ti	0.033	0.056	0.033	0.026	0.033	0.035	0.033	0.02	0.039	0.049
Al	0.195	0.329	0.234	0.117	0.295	0.335	0.261	0.139	0.229	0.295
Fe^{3+}	0.061	0.127	0.094	0.07	0.13	0.094	0.105	0.026	0.077	0.125
Fe^{2+}	0.181	0.139	0.146	0.185	0.199	0.124	0.143	0.188	0.18	0.114
Mn	0.006	0.006	0.005	0.009	0.012	0.004	0.006	0.005	0.007	0.008
Mg	0.79	0.68	0.75	0.794	0.6	0.728	0.756	0.836	0.735	0.712
Ca	0.884	0.892	0.888	0.871	0.917	0.913	0.878	0.874	0.891	0.904
Na	/	0.026	0.02	0.016	0.018	/	0.007	/	0.017	0.013
K	0.006	0.009	0.008	0.01	0.01	0.008	0.012	0.008	0.004	0.009
Al^{IV}	0.160	0.268	0.187	0.110	0.236	0.249	0.210	0.100	0.185	0.251
Al^{VI}	0.035	0.061	0.047	0.007	0.059	0.086	0.051	0.039	0.044	0.044
Mg#	71	73	74	71	63	77	75	71	70	78
Wollastonite	0.378	0.34	0.367	0.394	0.357	0.349	0.351	0.397	0.373	0.351
Enstatite	0.395	0.34	0.375	0.399	0.307	0.364	0.379	0.418	0.368	0.364
Ferrosilite	0.09	0.07	0.073	0.093	0.099	0.062	0.072	0.094	0.09	0.057
Others	0.136	0.251	0.185	0.113	0.238	0.224	0.199	0.09	0.169	0.228

Nb, negative anomalies for La and Zr, and very low Cr abundance (Fig. 4).

Olivine is weakly zoned ($Fo_{79–70}$), with negligible tephroite and monticellite components. Its forsterite contents are slightly higher than in SE–PL olivine, in accordance with what was defined by Clocchiatti at al. (2004; Fig. 4) for olivine in 2001 lavas.

Ti-magnetite is made up of Mt 47–65 mol% and Usp 35–56 mol%. TiO_2 and MgO contents are 12.2 wt.% and 3.4 wt.% respectively, with Al_2O_3 (4.8–5.8 wt.%) slightly lower than in SE–PL Ti-magnetite.

On the grounds of the time sequence and vents location of the eruption, the C–L samples have been grouped in Early C–L (EC–L) and Late C–L (LC–L) showing slight but significant chemical differences (see below). Phenocryst chemistry and modal proportions in the two groups are, however, quite similar. This can be explained considering that the distinction between these groups developed after the phenocryst phases were formed, involving only the residual melt.

C–L lavas and tephra have also been characterized by the frequent presence of quartzite xenoliths, with a mosaic granular structure and interstitial silica-rich glass (Corsaro et al., 2004).

4.2. SE–PL and C–L bulk rock compositions

The Total Alkali–Silica diagram shows that the rocks from the 2001 eruption are plotted in the field of the Etnean alkaline suite (Fig. 5A; Le Maitre, 1989). They are, however, less sodic than common Etnean rocks, as shown by their K_2O being higher than (Na_2O–2), by which they may be defined as

Table 4
Selected trace element concentrations in clinopyroxene phenocrysts at core and rim of EC–L, LC–L and SE–PL lavas

Sample	5.2A1	5.2A4	10.2A1	10.2A3	33.2A1	33.2A2	34.2A1	34.2A2	35.2A1	35.2A3
Location	EC–L	EC–L	EC–L	EC–L	LC–L	LC–L	LC–L	LC–L	SE–PL	SE–PL
Position	CORE	RIM	CORE	RIM	CORE	RIM	CORE	CORE	CORE	RIM
Li	0.5	0.8	5	14	0.7	0.3	1.2	1.9	1.3	1.3
Sc	101	68	105	113	142	114	66	66	91	90
V	281	271	339	376	352	324	268	277	322	318
Cr	147	82	20	100	756	519	34	48	12	10
Co	39	40	39	41	42	41	42	42	42	41
Sr	128	131	129	144	116.3	122	117	137	131	128
Y	25.6	16.3	28	28	18.52	13.07	23	25	24	22
Zr	90	61	122	111	95.97	51.87	81	96	96	93
Nb	0.81	0.43	0.8	0.7	0.8	0.37	0.62	0.76	0.65	0.62
Ba	0.09	0.13	0.12	/	0.16	0.05	0.11	0.064	0.078	0.08
La	12.1	5.8	14.8	14.4	8.14	4.8	9.7	10	13.2	12.9
Ce	41.4	20.3	48.4	48.6	29.36	17.59	35.5	37	46.5	46.1
Pr	6.4	3.6	7.5	7.5	4.89	3.04	5.9	6.2	7.3	7.1
Nd	33.4	19	36.5	36.8	25.95	16.84	30.3	31.9	36.8	35.9
Sm	8.2	5.1	9.4	9.5	7.16	4.85	8	8.2	9.4	9.1
Eu	2.56	1.69	2.9	3.2	2.43	1.72	2.6	2.71	3	2.9
Gd	6.6	4.1	7.7	8.1	6.35	4.14	6.4	6.8	7.8	7.6
Tb	0.96	0.68	1.2	1.27	0.99	0.64	1.03	1.03	1.18	1.15
Dy	5.0	3.5	5.8	6.4	4.98	3.3	5.1	5.3	6.0	5.8
Ho	0.87	0.6	1.07	1.11	0.92	0.61	0.97	0.99	1.09	1.04
Er	1.91	1.4	2.42	2.48	1.97	1.26	2.23	2.16	2.29	2.26
Tm	0.25	0.18	0.32	0.33	0.26	0.17	0.3	0.29	0.32	0.3
Yb	1.64	1.04	2.07	2.07	1.62	0.98	1.84	1.86	1.9	1.7
Lu	0.23	0.14	0.29	0.29	0.22	0.13	0.23	0.25	0.27	0.25
Hf	2.8	2.1	4.1	4.2	4.23	2.19	2.9	3.2	3.6	3.3
Ta	0.09	0.07	0.11	0.13	0.16	0.06	0.1	0.11	0.11	0.1
Pb	0.08	0.06	0.09	0.09	0.04	0.04	0.08	0.09	0.11	0.1
Th	0.15	0.074	0.17	0.18	0.16	0.06	0.12	0.12	0.16	0.14
U	0.021	0.013	0.028	0.021	0.02	0.01	0.02	0.021	0.022	0.019

mildly potassic (Fig. 5B; Le Maitre, 1989). On the whole, the rocks are then potassic trachybasalts, except for two C–L samples, with Alk <5%, erupted at the 2100 m vent of the C–L system, that may be defined as basalts (Table 7).

The primordial mantle (Wood et al., 1979) normalized spider diagrams confirm that minor element compositions of the sampled rocks are generally consistent to those of the basic members of the Etnean alkaline sequence. In detail, they are intermediate between the within plate basalts (WPB) and calc-alkaline basalts (CAB), as defined by Sun (1980) and Pearce (1982). Elements such as Rb, Ba, Th, U and K are enriched in the Etnean rocks compared to the average WPB, whereas Ta, Ti and Nb are less abundant than in common WPB, therefore partly recalling a CAB pattern.

Chondrite normalized (Anders and Ebihara, 1982) REE patterns are markedly homogeneous, with a clear overall fractionation (La_N/Yb_N=15–17), and little negative Eu anomaly (Eu_N/Eu^*=0.89–0.98); LREE are more fractionated than HREE (La_N/Sm_N=3.6–4.0; Gd_N/Yb_N=2.7–3.1). On the whole, the pattern is similar to that of the Etnean alkaline suite (Cristofolini et al., 1981, 1984, 1988, 1991; Barbieri et al., 1993; Corsaro and Cristofolini, 1993, 1996; Tanguy et al., 1997) (Table 8).

In spite of their petrographic differences, SE–PL and C–L rocks show an overall limited variability in major and minor element concentrations, with SiO_2 contents in the range 49–51 wt.%. A careful examination of their variation patterns, however, points out regular changes of the sampled rocks, related to space and time. In particular, the EC–L ones are slightly

Table 5
Selected major element concentrations in Mg-hastingsite phenocrysts in EC–L and LC–L lavas

Sample	5.2A1	17.2A2
Location	EC–L	LC–L
SiO_2	41.77	41.55
TiO_2	3.04	3.14
Cr_2O_3	0.21	0.16
Al_2O_3	13.50	13.26
FeO	11.42	11.54
MnO	0.23	0.26
MgO	13.73	13.45
NiO	/	0.09
CaO	11.98	11.85
Na_2O	1.69	1.46
K_2O	0.87	0.95
Total	98.44	97.71
Si	5.835	5.854
Ti	0.319	0.333
Cr	0.023	0.018
Al	2.222	2.202
Fe^{2+}	1.334	1.360
Mn	0.027	0.031
Mg	2.859	2.824
Ni	/	0.01
Ca	1.793	1.789
Na	0.458	0.399
K	0.155	0.171
OH	2	2

more acid and very homogeneous in their compositions, compared to the LC–L lavas, which are more basic and heterogeneous, resembling the SE–PL lavas (Figs. 6 and 7).

5. Discussion

5.1. Erupted magmas

Simultaneous eruptions from distinct vents are not rare in the historical records on Mount Etna. Typically "bi-radial" adventive eruptions are cases in which magmas rise through the main conduit system to be drained along radial or rift structures only at a shallow level (Romano and Sturiale, 1982). The 2001 eruption, however, occurred within the same narrow sector on the southern flank of the volcano and data show that three distinct magmas were involved: i) the SE–PL magma that erupted from NNW–SSE trending fractures on the high southern flank (2650–3100 m a.s.l.) of the volcanic edifice; ii) the EC–L magma erupted at lower elevations (2100 m a.s.l.) on the same flank from N–S trending fractures; iii) the slightly different LC–L magma, erupted later from vents at intermediate elevation (2550 m a.s.l.).

All of them are mildly potassic trachybasalts and their plagioclase and clinopyroxene cores have the same REE and minor element contents, supporting the idea of their cognate origin, but appear as fractionated from parent basalts under different physical conditions. SE–PL lavas are porphyritic (P.I. 30–40) with prevailing plagioclase, whereas EC–L and LC–L lavas are mesophyric (P.I. 10–20) with plagioclase and augite in similar amounts and up to 6 vol.% of Mg-hastingsite among the phenocrysts.

Table 6
Selected trace element concentrations in Mg-hastingsite phenocrysts in EC–L and LC–L lavas

Sample	5.2A1	17.2A2
Location	EC–L	LC–L
Li	21	4
Sc	61	55
V	484	550
Cr	4	16
Co	59	67
Rb	3.2	3
Sr	699	605
Y	34	37
Zr	102	115
Nb	44	55
Ba	391	340
La	20.8	22.5
Ce	74.4	81.3
Pr	10.8	12.2
Nd	52.5	61.7
Sm	12	14.4
Eu	4.3	4.7
Gd	10.1	11.2
Tb	1.55	1.82
Dy	7.7	8.8
Ho	1.37	1.73
Er	3.1	3.6
Tm	0.4	0.5
Yb	2.64	3
Lu	0.3	0.42
Hf	3.6	4.1
Ta	1.7	1.8
Pb	0.66	0.66
Th	0.23	0.21
U	0.048	0.054

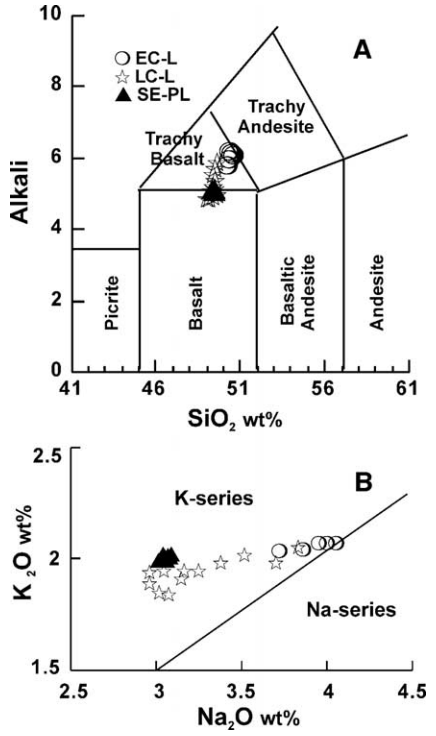

Fig. 5. A) Total Alkali vs. Silica (TAS) diagram (Le Maitre, 1989); SE–PL lavas are distributed at the basalt–trachybasalt boundary, whereas EC–L markedly fall in the trachybasalt field near to trachyandesite field; LC–L lavas are aligned between the two groups. B) Na_2O vs. K_2O (wt.%) diagram (Le Maitre, 1989); SE–PL rocks fall in the potassic field; EC–L show a distinctly more sodic character; LC–L lavas appear as intermediate between the two groups. Symbols same as in Fig. 3.

SE–PL features are consistent with those of the Etnean rocks of summit and subterminal activity in the last few decades. Here, magma differentiation is driven by polybaric crystallization of plagioclase/mafic phases, mostly controlled by gas migration and selective fractionation. The steady degassing conditions in an open and repeatedly filled conduit, prevent the partial pressure increase and allow a concentration gradient of the volatile components above the saturation level. In these conditions, fractionation effects are compensated by continuous magma input from depth. Large rhythmically zoned plagioclase crystals, abundantly found on Etnean lavas, are typically produced in such a dynamic degassing system (cf. Cashman, 1990; Higgins and Roberge, 2003; Couch et al., 2003a,b).

In EC–L and LC–L volcanics the presence of Mg-hastingsite phenocrysts and An-enriched plagioclase rims is evidence for high volatile pressure within a closed system. Dehydration rims of phenocrysts are related to decompression and consequent volatile loss immediately preceding and during the eruption.

The outer rims of plagioclase and clinopyroxene in SE–PL lavas preserve compositions similar to the cores; conversely, clinopyroxene and plagioclase phenocrysts in EC–L and LC–L products are rimmed by envelopes that are significantly depleted in RE and other minor elements. This suggests that, after the core nucleation, physical conditions controlling the crystallization must have changed. A plausible hypothesis is that this occurred due to the onset of a new phase with higher distribution coefficients (K_D) for REE than clinopyroxene: petrographic evidence strongly suggests Mg-hastingsite as this new phase.

The presence of amphibole sets some constraints on P–T conditions in the C–L magma batch. An interesting analogue is provided by some experimental results (Foden and Green, 1992; Holloway and Blank, 1994; Rutherford and Devine, 2003) showing Mg-hastingsite coexisting with a high- alumina basalt melt at T ~980 °C, for $P_{tot}=P_{H20}=0.2$ GPa.

This pressure may be inferred at a depth of about 6 km, where the C–L magma may be assumed to have resided in accord with the deepest hypocentres (Monaco et al., 2005). The crystallization of Mg-hastingsite would therefore require an equilibrium T ~980 °C, lower than the commonly measured T in most of the Etnean lavas (cf. Pompilio et al., 1998).

5.2. Deep basic end-member

LC–L rocks sampled at the Laghetto vent, are chemically distinct from the EC–L ones which erupted at the Calcarazzi area. LC–L products are plotted along a tie-line between the average composition of EC–L lavas and a hypothetical deep basic magma (DBM), not erupted in the 2001 event, which should have risen, relatively undegassed, through a system that was independent from the main conduit (Figs. 6–8; Table 7). The DBM major and minor composition has been estimated as similar to the average of the oligophyric trachybasalts, considered to be among the least differentiated Etnean alkaline rocks (Armienti et

Table 7
Major element compositions (water free) of some representative EC–L, LC–L and SE–PL lavas; the composition of the hypothetical DBM has also been reported

Sample	1EC–L	5EC–L	6LC–L	10LC–L	17LC–L	1SE–PL	3SE–PL	DBM
SiO_2	50.26	50.67	49.35	49.62	49.06	49.38	49.48	47.92
TiO_2	1.46	1.36	1.60	1.46	1.62	1.66	1.68	1.80
Al_2O_3	16.92	17.28	16.82	17.15	16.14	16.84	16.58	15.80
Fe_2O_3	9.49	8.67	10.29	9.32	10.86	10.49	10.65	11.50
MgO	5.63	5.61	5.75	5.69	6.44	5.34	5.25	7.00
MnO	0.17	0.16	0.18	0.17	0.19	0.19	0.19	0.18
CaO	9.78	9.67	10.52	10.16	10.41	10.55	10.70	11.30
Na_2O	3.73	3.96	3.15	3.84	2.97	3.09	3.03	2.70
K_2O	2.03	2.07	1.91	2.05	1.89	2.02	2.00	1.50
P_2O_5	0.53	0.53	0.44	0.53	0.43	0.44	0.44	0.30
Mg#	50	48	51	50	52	45	44	/

Table 8
Trace element data of some representative EC–L, LC–L and SE–PL lavas

Sample	1EC–L	5EC–L	6LC–L	10LC–L	17LC–L	1SE–PL	3SE–PL
Ba	568	583	549	586	531	601	596
Ce	108	111	103	111	101	111	109
Co	35.3	36.7	37.1	37.8	39.5	34.6	34.2
Cr	38	35	37	40	36	28	25
Cu	118	116	128	146	125	136	125
Dy	5.33	5.29	5.14	5.73	5.08	5.46	5.31
Er	2.45	2.63	2.65	2.64	2.44	2.61	2.65
Eu	2.54	2.81	2.57	2.85	2.66	2.76	2.73
Ga	19	20	20	21	19	20	19
Gd	8.09	8.37	8.16	8.57	8.01	8.33	8.24
Hf	5	5	5	5	5	5	5
Ho	0.96	1.03	0.97	1.04	0.97	0.99	1.01
La	55.4	57.1	52.1	56.5	51.6	56.6	56.0
Lu	0.31	0.35	0.32	0.33	0.31	0.31	0.32
Nb	42	44	40	42	39	43	43
Nd	46.4	48.0	44.6	48.4	44	47.1	47.5
Ni	32	32	32	40	42	33	26
Pr	12.0	12.6	11.6	12.6	11.6	12.5	12.4
Rb	46.1	48.0	46.6	49.3	45.5	46.2	47.2
Sc	26	26	27	27	28	25	25
Sm	9.0	9.1	8.5	9.3	8.5	9.3	9.1
Sr	1060	1100	1070	1110	1030	1120	1110
Ta	2.4	2.5	2.2	2.3	2.3	2.4	2.4
Tb	1.09	1.14	1.12	1.16	1.07	1.10	1.11
Th	8.6	8.6	7.8	8.5	7.9	8.3	8.3
Tm	0.35	0.35	0.32	0.38	0.33	0.34	0.36
U	2.21	2.32	2.05	2.15	2.01	2.19	2.18
V	282	294	295	310	291	291	293
Y	24.5	25.4	25.0	26.4	24.4	25.4	25.5
Yb	2.1	2.3	2.2	2.3	2.1	2.3	2.2
Zn	83	85	86	90	84	88	85
Zr	199	203	187	201	186	198	207

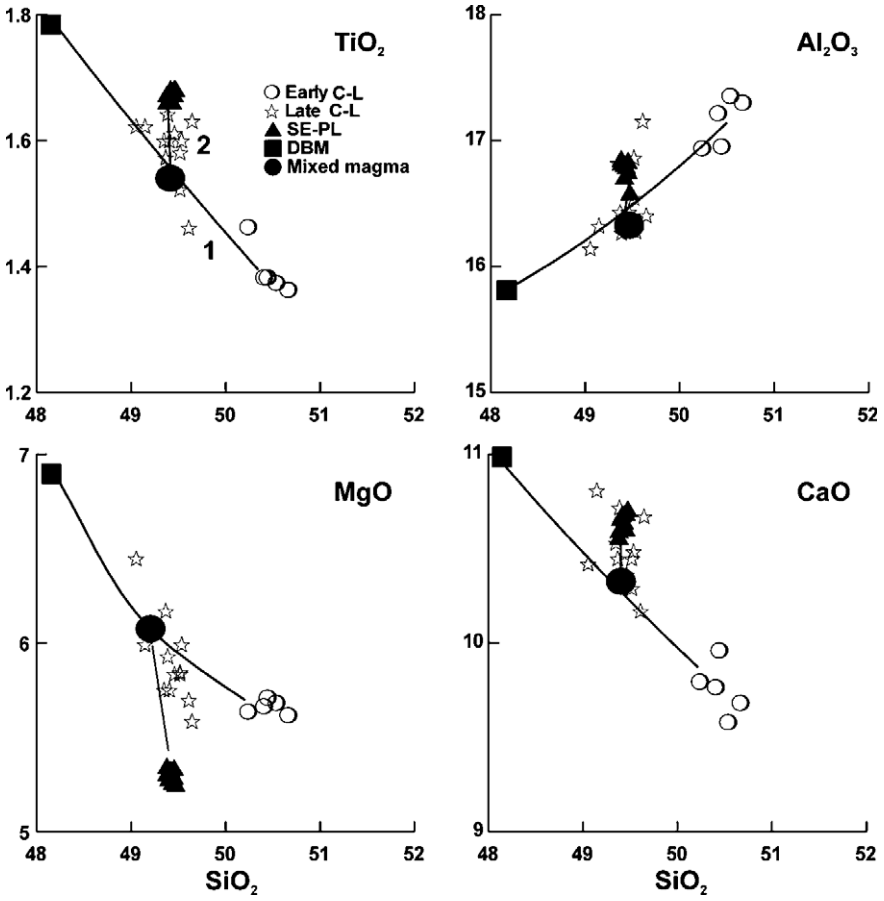

Fig. 6. Selected major elements abundances (wt.%) vs. SiO_2 (wt.%). Three groups of samples, erupted at different vents, Early C–L, Late C–L and SE–PL lavas, have distinct features (See Discussion in the text). LC–L lavas clearly differ from EC–L lavas. The most mafic members of the LC–L group are plotted along a line (tie-line 1) connecting the EC–L lavas and an inferred Deep Basic Magma (DBM), which is consistent with mixing of the two end members. Other LC–L lavas shift toward the SE–PL field, possibly due to a limited mixing with the SE–PL magma at the intersection of the two fracture systems near to the surface. Symbols same as in Fig. 3.

al., 1988, 1989), whose major element composition could also be quantitatively obtained by subtracting ~10% of solid phases, mainly clinopyroxene+Ti-magnetite, olivine and plagioclase from DBM (XLFRAC).

According to Treuil and Joron (1975; Fig. 8A–B) the LC–L compositions may not be related to the DBM and EC–L ones by crystal fractionation. Furthermore the actual alignment may not be accounted for by different degrees of partial melting, because the C–L compositions do not represent primary melts (Mg#<56; SiO_2>49 wt.%). The tie-line trend could then be related to mixing varying proportions of the EC–L end-member with DBM.

The presence of a primitive and volatile enriched magma like DBM, characterized by the fractionation of hyperstene within the feeding system of 2001 event, has also been inferred by Clocchiatti et al. (2004). A DBM temperature of ~1150 °C was obtained using the regression curves from data on glasses of Etnean hawaiites and alkali basalts (cf. Pinkerton and Norton, 1995; Pompilio et al., 1998).

5.3. Modelling the magma mixing

As suggested above, mixing occurred between the Mg-hastingsite-bearing magma (C–L), residing in a closed batch, and an inferred DBM, whereas the SE–

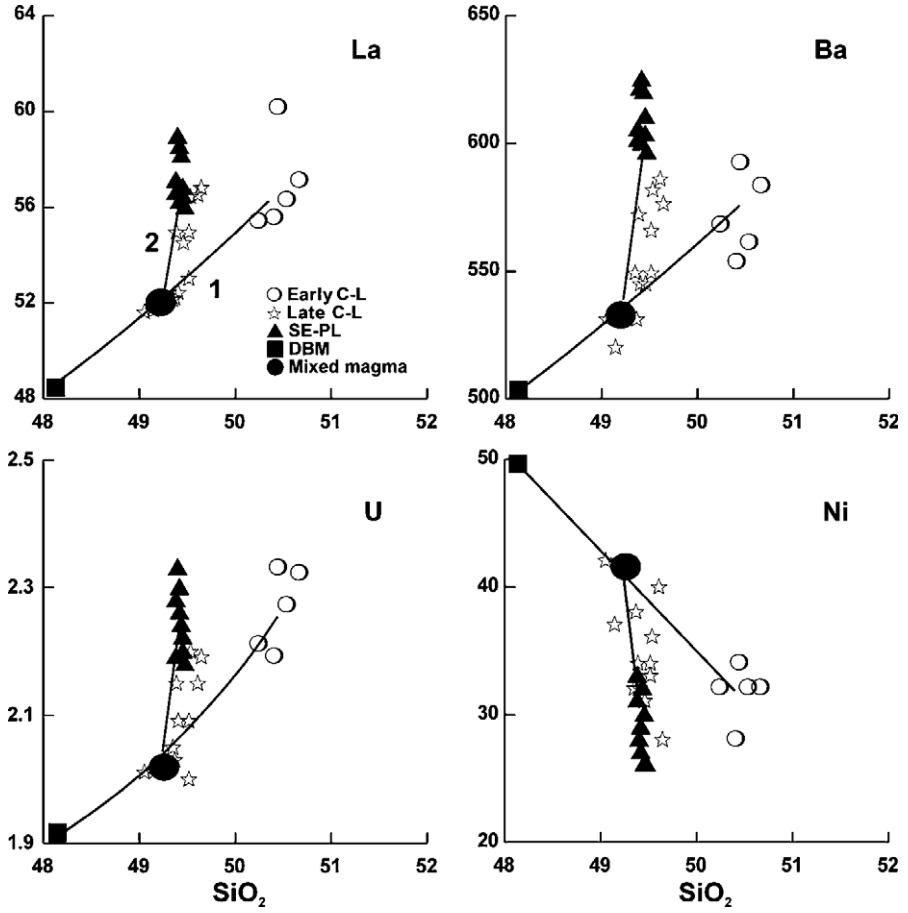

Fig. 7. Selected incompatible (La, Ba, U) and compatible (Ni) trace elements abundances (ppm) vs. SiO_2 (wt.%) for Early C–L, Late C–L and SE–PL lavas. Distribution patterns are similar to those shown by major elements. See Fig. 3 for symbols.

PL magma should have played no significant role in the mixing process, as suggested by the marked differences between the textures and mafic to salic phenocryst ratios of LC–L and SE–PL. However, the alignment of data points of LC–L lavas toward the SE–PL field (Figs. 6 and 7) suggests that a modest interaction might have occurred.

Mixing had to occur at the level of the C–L batch, immediately before and/or during the start of C–L magma ascent. It may also be inferred that after the first seismic swarm (July 17th) DBM rose up, intersected the batch and uprise system of the C–L magma, and partially mixed with it. Mixing between the relatively cool C–L magma (T_{equil} of Mg-hastingsite ~980 °C) and the hotter DBM (T ~1150 °C) set off a limited heat transfer (see Appendix). The increased T of the mixed LC–L magma must have lowered the volatile solubility, increasing the gas exsolution rate and enhancing the amphibole breakdown (cf. Johnson et al., 1994; Lange, 1994). The physical disturbance originated by DBM entering the C–L shallow reservoir probably contributed in easing the gas exsolution.

The LC–L magma supplied a significant amount of gas, characterizing then the dynamics of the eruptive activity at the Laghetto vent, which was on the whole highly explosive. The very first eruptive phase at the Laghetto vent was dominantly phreato-magmatic, as expected considering the presence of shallow groundwater reservoirs (Coltelli et al., 2001; Taddeucci et al., 2002, 2004; Behncke and Neri, 2003). The explosive activity at the

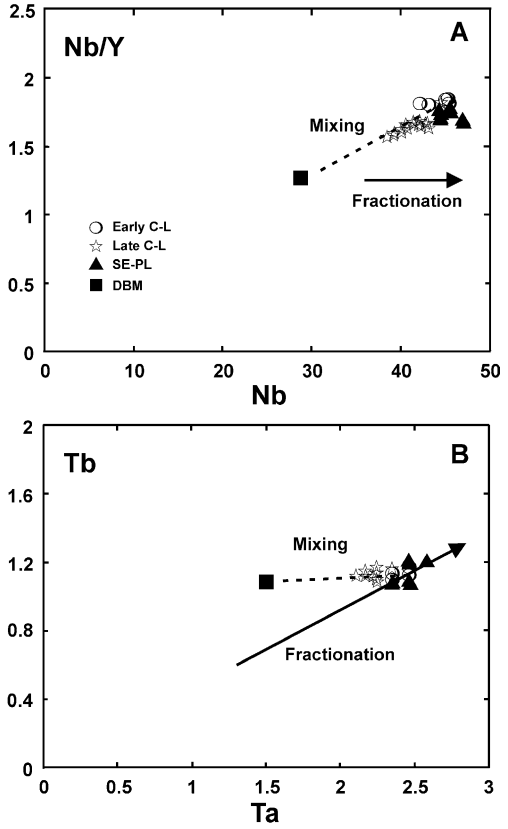

Fig. 8. Nb/Y vs. Nb and Tb vs. Ta diagrams (Treuil and Joron, 1975). See Discussion in the text. Symbols same as in Fig. 3.

Laghetto vent, however, went on after the phreatomagmatic phase with the involvement of merely magmatic juvenile gases (Clocchiatti et al., 2004), with an explosivity index higher than 30%, which is quite uncommon for the historically recorded Etnean activity (cf. Romano and Sturiale, 1982; Busà et al., 1997). The continued eruption of lavas with EC–L compositions, from the lower vent, at the Calcarazzi area, was mostly effusive and produced a considerably lower amount of tephra. This makes it likely that the main reason for the explosive eruptive behaviour at the Laghetto vent might be related to the efficient degassing resulting from the mixed nature of the LC–L magma.

5.4. Interpreting the eruption course

The seismic swarm occurred between July 12th and 15th affected the upper 6 km of the crust beneath the summit craters. On July 13th the eruption began with the first lava fountaining at the South-East crater. The seismic swarm could be related to an intense fracturing of the volcanic edifice and its basement, which originated the development of the SE–PL fissures, trending NNW–SSE, at the surface (Fig. 9, phase 1).

From July 15th to 20th the earthquake hypocentres, still concentrated within the upper 6 km of the crust, shifted southwards underneath the Piano del Lago and Calcarazzi areas. The seismic pattern was characterized by a gradual disappearance of the deeper seismic foci. This second seismic swarm could be associated with the opening of C–L fractures directed N–S at the surface, and produced the sudden decompression of the C–L magma, residing at depth. This gave rise to gas exsolution in the magma, and triggered its ascent to the surface; the associated disappearance of the deeper quakes may be related to the progressive fracture filling by the C–L magma. The eruption at the Calcarazzi area started at the end of the seismic swarm during the night of July 18th (Fig. 9, phase 2).

On July 21st the NNW–SSE trending SE–PL fissure belt extended downslope to the Laghetto area (Fig. 1) where it intersected the N–S oriented C–L fractures, that in the meanwhile prolonged northward from the Calcarazzi area. DBM probably rose up next to the surface at the southern end of the NNW–SSE trending system and not along the N–S system. This can be inferred by the very fact that only EC–L lavas erupted from the N–S oriented fracture system, whereas the LC–L ones erupted where and when the two SE–PL and C–L tectonic systems intersected. At the intersection fractures grew then wider and originated a pit crater where the mixed magma LC–L explosively erupted (Fig. 9, phase 3). Mixing of DBM with the original C–L magma should have started at the level of the C–L batch; the evolution of the seismic pattern does not indicate, however, if mixing had occurred before or during the shallow fracture opening. The timing and space development of the eruption makes it clear how the development of local tectonic phenomena in the volcanic edifice and in the crust immediately underneath strongly controlled the eruptive mechanisms.

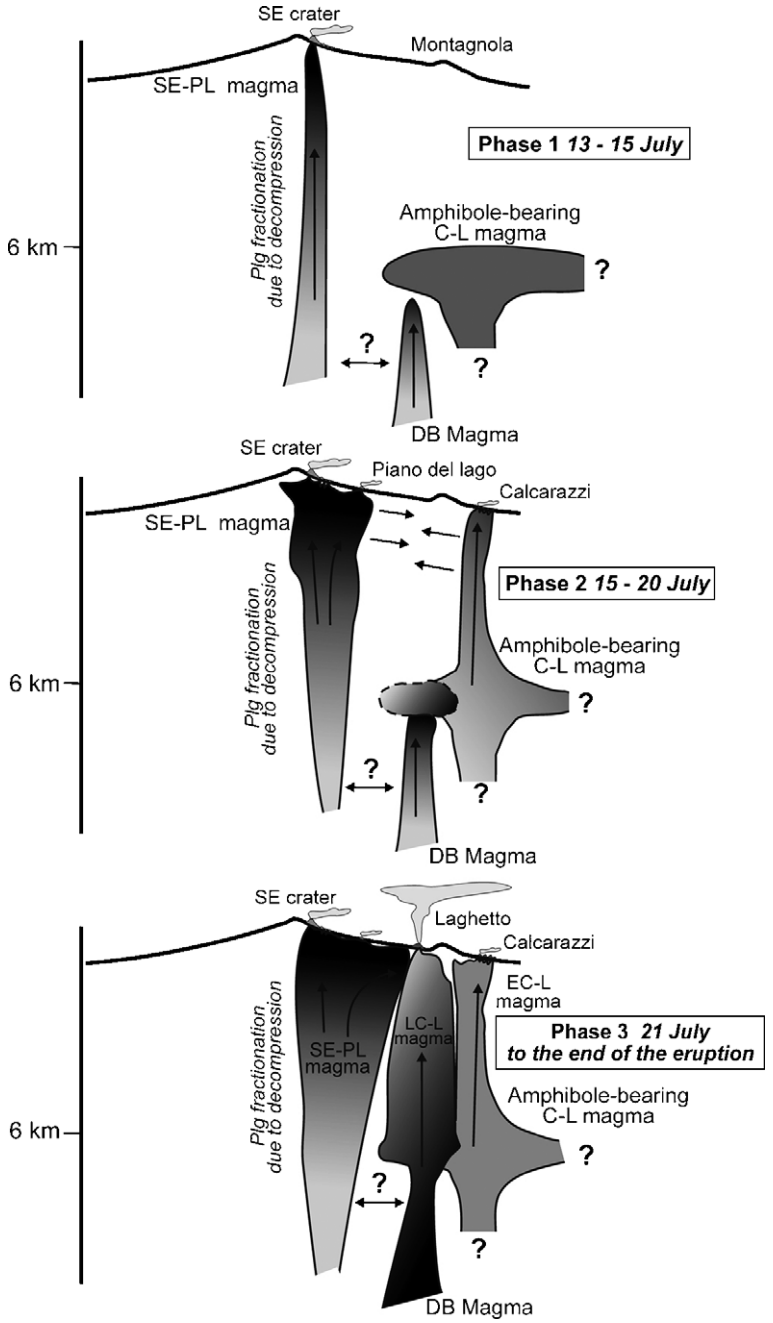

Fig. 9. Cartoon of the evolution of the July–August 2001 eruption illustrating its three main phases: Phase 1) first seismic crisis, opening of NNW–SSE oriented SE–PL fractures and eruption of SE–PL trachybasaltic magma at the South-East crater; Phase 2) second seismic crisis, widening of the SE–PL fractures and eruption of trachybasaltic magma at Piano del Lago; opening of the N–S oriented fractures system and eruption of the EC–L Mg-hastingsite-bearing magma at the 2100 m vent; interaction and mixing of DBM with the residing EC–L magma; small arrows indicate the direction of the fractures expansion; Phase 3) SE–PL and C–L ground fracture systems intersect at the Laghetto area, originating a pit crater, and the mixed LC–L magma is erupted with high explosivity.

6. Conclusions

The 2001 eruptive event has been extensively studied by many authors, who pointed out an origin of the erupted products from distinct magmas, as well as the abnormally large explosivity of the eruptive phenomena. Great emphasis was also put on the presence of amphibole megacrysts in one type of the lavas, which was considered very peculiar, and on the interpretation of the seismic and tectonic behaviour. Relatively little attention was paid in the understanding of the eruptive dynamics and the relationship between different magmas. Here, the eruptive evolution and the geochemistry of the erupted products have been examined jointly.

The eruptive phenomena developed under the control of the fast uprise, within a few days, of distinct magmas (SE–PL and C–L) either through the central feeding system and connected fractures (directed NNW–SSE; 3040–2700 m a.s.l.), or newly opened fractures (directed N–S; 2550–2100 m a.s.l.) in the volcanic edifice and in the crust immediately underneath.

Clear geochemical evidence supports the existence of a basic magma (DBM), which did not erupt, but nevertheless rose through the NNW–SSE fracture system next to its intersection with the N–S one, and partly mixed with the amphibole-bearing C–L magma within its batch. The consequence of this has been important in enhancing the most intensely explosive phase during the 2001 event.

Mechanisms of the same kind have been extensively discussed in a great deal of references, mainly as a proper eruptive trigger for stratovolcanoes with andesitic or more acid compositions. In most of the studied cases this occurred when markedly different members were involved (e.g. basaltic-andesitic input into a rhyodacitic body) (Calderone et al., 1990; Morrissey and Chouet, 1997; Snyder, 1997; Venezky and Rutherford, 1997; Woods and Cardoso, 1997; Folch and Marti, 1998; Hort, 1998; Linde and Sacks, 1998; Murphy et al., 1998; Scaillet and Evans, 1999; Leonard et al., 2002; Nakagawa et al., 2002, Phillips and Woods, 2002; Thornber et al., 2003). In the present instance both magmas have basic compositions and the critical factors affecting the eruptive mechanism are to be looked for among the physico-chemical parameters: pressure, temperature, and volatile content and solubility in the melt. This casts a new light for interpreting similar eruptions in "basaltic" volcanoes and answering some problems related to eruptions with uncommonly high explosivity, even when only basic magmas are involved.

Acknowledgements

The authors are grateful to D. La Rocca and E. Giuffrida (Dipartimento di Scienze Geologiche, University of Catania) for their assistance in XRF data acquisition, to L. Negretti (Dip.Te.Ris, University of Genoa) for her help in EPM analyses and to A. Zanetti (CNR-Dipartimento di Geoscienze e Georisorse, Pavia) for his technical assistance in LAM ICP-MS data acquisition. Careful revision of the English text by Dr. Karen Ebersold is gratefully acknowledged.

The analytical work for this paper was made possible by DR78 grants of the University of Genoa to L. Cortesogno.

Appendix A. Magma mixing effects on the eruptive dynamics

An assessment of heat transferred in the mixing process may be found by computing the molar specific heat (Cp) for the components of the two involved magmas (Table 7):

$$\mathrm{Cp}_{\mathrm{EC-L}} = \Sigma_i \chi_i \mathrm{Cp}_{i,\,\mathrm{EC-L}}$$

$$\mathrm{Cp}_{\mathrm{DBM}} = \Sigma_i \chi_i \mathrm{Cp}_{i,\,\mathrm{DBM}}$$

where χ_i is the molar fraction of the i component in the melt and Cp_i is the specific heat of the oxide i; Cp values were calculated by the following equation (Richet and Bottinga, 1985):

$$\mathrm{Cp}_{\mathrm{melt}} = \Sigma_i \chi_i \left(K_{1i} + K_{2i}T + K_{3i}T^{-2}\right)$$

where $K_{n,i}$ are parameters for the calculation of heat capacity in silicatic melts.

The results are then:

$$Cp_{EC-L} = 101\ J/molK$$

$$Cp_{DBM} = 105\ J/molK$$

The enthalpic difference ΔH_i for the two magmas – found integrating between the reference temperature T_r (298, 15 K standard status) and T_{EC-L} – is:

$$\Delta H_{EC-L} = Cp_{EC-L}(T_{EC-L} - T_r) = 96\,KJ/mol$$

$$\Delta H_{DBM} = Cp_{DBM}(T_{DBM} - T_r) = 119\,KJ/mol$$

$$\Delta H_{mixing} = \Delta H_{DBM} - \Delta H_{EC-L} = 5\,KJ/mol$$

Some assumptions were made to perform the calculations, the most relevant of which is that the involved magmas were both completely molten; this is obviously not true since their P.I. was at least 10–20, according to the petrographic evidence. Although this assumption could appear as unrealistic, it is however to be considered that the crystallized phases do not show significant reaction structures related to the varied T and melt composition.

As heat transfers from higher to lower H systems, mixing supplied heat to the original EC–L component, increasing its T, because very little of this energy was consumed by endothermic reactions (amphibole breakdown, mineral resorption, etc.).

Provided that all of the heat produced in the mixing process is used for increasing T of EC–L, and that the molar ratio X_{EC-L}/X_{DBM} is not less than 3 (X_{EC-L}= 0.75; X_{DBM}=0.25; see Fig. 8), T_{equil} may be calculated by the Russel equation (1990) as:

$$T_{equil} = (X_{DBM}\,Cp_{DBM}\,T_{DBM}) + (X_{EC-L}\,Cp_{EC-L}\,T_{EC-L}) / X_{EC-L}\,Cp_{EC-L} + X_{DBM}\,Cp_{DBM}$$

For T_{EC-L}=1253 K and T_{DBM}=1423 K the resulting T_{equil} is 1297 K (~1025 °C).

References

Acocella, V., Neri, M., 2003. What makes flank eruptions? The 2001 Etna eruption and its possible triggering mechanisms. Bull. Volcanol. 65, 517–529.

Alparone, S., Andronico, D., Giammanco, S., Lodato, L., 2004. A multidisciplinary approach to detect active pathways for magma migration and eruption at Mt. Etna (Sicily, Italy) before the 2001 and 2002–2003 eruptions. J. Volcanol. Geotherm. Res. 136, 121–140.

Anders, E., Ebihara, M., 1982. Solar system abundances of the elements. Geochim. Cosmochim. Acta 46, 2363–2380.

Armienti, P., Innocenti, F., Petrini, R., Pompilio, M., Villari, L., 1988. Sub-aphyric alkali basalt from Mt. Etna: inferences on the depth and composition of the source magma. Rend. Soc. Ital. Mineral. Petrol. 43, 877–891.

Armienti, P., Innocenti, F., Petrini, R., Pompilio, M., Villari, L., 1989. Petrology and Sr-Nd isotope geochemistry of recent lavas from Mt. Etna — bearing on the volcano feeding system. J. Volcanol. Geotherm. Res. 39, 315–327.

Barbieri, M., Cristofolini, R., Delitala, M.C., Fornaseri, M., Romano, R., Taddeucci, A., Tolomeo, L., 1993. Geochemical and Sr-isotope data on historic lavas of Mount Etna. J. Volcanol. Geotherm. Res. 56 (1–2), 57–69.

Behncke, B., Neri, M., 2003. The July–August 2001 eruption of Mt. Etna (Sicily). Bull. Volcanol. 65, 461–476.

Billi, A., Acocella, V., Funiciello, R., Giordano, G., Lanzafame, G., Neri, M., 2003. Mechanism for ground-surface fracturing and incipient slope failure associated with the 2001 eruption of Mt. Etna, Italy: analysis of ephemeral field data. J. Volcanol. Geotherm. Res. 22, 281–294.

Bonaccorso, A., Aloisi, M., Mattia, M., 2002. Dike emplacement forerunning the Etna July 2001 eruption modelled through continuous tilt and GPS data. Geophys. Res. Lett. 29 (2), 1–4.

Bottazzi, P., Tiepolo, M., Vannucci, R., Zanetti, A., Brumm, R., Foley, S.F., Oberti, R., 1999. Distinct sites preferences for heavy and light REE in amphibole and the prediction of $^{amph/L}D_{REE}$. Contrib. Mineral. Petrol. 137, 36–45.

Busà, T., Calderone, G., Cristofolini, R., Frazzetta, G., 1997. New evidence for explosive activity on Mt. Etna over the last 50 kyr. Per. Mineral. 66, 287–301.

Calderone, G.M., Gronvold, K., Oskarsson, N., 1990. The welded air-fall tuff layer at Krafla, northern Iceland: a composite eruption triggered by injection of basaltic magma. J. Volcanol. Geotherm. Res. 44, 303–314.

Calvari, S., Pinkerton, H., 2004. Birth, growth and morphologic evolution of the "Laghetto" cinder cone during the 2001 Etna eruption. J. Volcanol. Geotherm. Res. 132, 225–239.

Cashman, K.V., 1990. Textural constraints on the kinetics of crystallization of igneous rocks. In: Nicholls, J., Russel, J.K. (Eds.), Modern Methods of Igneous Petrology: Understanding Magmatic Processes, Rev. Mineral., vol. 24, pp. 259–314.

Clocchiatti, R., Tanguy, J.C., 2001. Amphibole megacrysts from the 2001 S-flank eruption, Etna, Italy. Bull. Glob. Volcanism Netw. 26 (10), 3–4.

Clocchiatti, R., Condomines, M., Guènot, N., Tanguy, J.C., 2004. Magma changes at Mount Etna: the 2001 and 2002–2003 eruptions. Earth Planet. Sci. Lett. 226, 397–414.

Coltelli, M., Del Carlo, P., Scollo, S., 2001. Physical parameters of the ash fallout occurred during the 2001 eruption of Etna and implication for volcanic hazard assessment. Proc. Ass. 1 Anno, GNV-INGV, Rome, pp. 241–242.

Corsaro, R.A., Cristofolini, R., 1993. Nuovi dati petrochimici ed isotopici sulla successione del Mongibello Recente (Mt Etna). Boll. Accad. Gioenia Sci. Nat. 341, 185–225.

Corsaro, R.A., Cristofolini, R., 1996. Origin and differentiation of recent basaltic magmas from Mount Etna. Mineral. Petrol. 57, 1–21.

Corsaro, R.A., Cristofolini, R., Ferlito, C., Mazzoleni, P., Miraglia, L., Viccaro, M., 2004. Gli xenoliti presenti nelle vulcaniti eruttate dall'Etna nel 2001, 2002–2003 e 2004. GNV-Protezione Civile General Assembly, Naples, 20–22 December 2004.

Couch, S., Harford, C.L., Sparks, R.S.J., Carroll, M.R., 2003. Experimental constraints on the conditions of formation of highly calcic plagioclase microlites at the Soufriere Hills Volcano, Montserrat. J. Petrol. 44, 1455–1475.

Couch, S., Sparks, R.S.J., Carroll, M.R., 2003. The kinetics of degassing-induced crystallization at Soufriere Hills Volcano, Montserrat. J. Petrol. 44, 1477–1502.

Cristofolini, R., Lo Giudice, A., 1969. Ricerche su due kaersutiti etnee. Atti. Acc. Gioenia Sci. Nat. 20, 181–193.

Cristofolini, R., Romano, R., 1982. Petrological features of Etnean volcanic rocks. Mem. Soc. Geol. Ital. 23, 99–115.

Cristofolini, R., Scribano, V., Tranchina, A., 1981. Interpretazione petrogenetica di variazioni composizionali in fenocristalli femici di lave etnee. Rend. Soc. Ital. Mineral. Petrol. 31, 309–336.

Cristofolini, R., Ghiara, M.R., Stanzione, D., Tranchina, A., 1984. Petrologic and geochemical features of rocks from recent eruption at Mt Etna, Sicily. Neues Jahrb. Mineral. Abh. 149 (3), 267–282.

Cristofolini, R., Puglisi, G., Scribano, V., Tranchina, A., 1988. Within and among flow petrological variations in a sample from dated eruptions of the last ten centuries on Mount Etna. Per. Mineral. 56, 1–24.

Cristofolini, R., Corsaro, R.A., Ferlito, C., 1991. Variazioni petrochimiche nella successione etnea: un riesame in base a nuovi dati da campioni di superficie e da sondaggi. Acta Vulcanol. 1, 25–37.

Foden, J.D., Green, D.H., 1992. Possible role of amphibole in the origin of andesite: some experimental and natural evidence. Contrib. Mineral. Petrol. 109, 479–493.

Folch, A., Marti, J., 1998. The generation of overpressure in felsic magma chambers by replenishment. Earth Planet. Sci. Lett. 163 (1–4), 301–314.

Franzini, M., Leoni, L., Saitta, M., 1972. A simple method to evaluate the matrix effect in x-ray fluorescence analysis. X-Ray Spectrom. 1, 151–154.

Gillot, P.Y., Kieffer, G., Romano, R., 1994. The evolution of Mount Etna in the light of potassium-argon dating. Acta Vulcanol. 5, 81–87.

Higgins, M.D., Roberge, J., 2003. Crystal size distribution of plagioclase and amphibole from Soufriere Hills Volcano, Montserrat: evidence for dynamic crystallization–textural coarsening cycles. J. Petrol. 44, 1401–1411.

Holloway, J.R., Blank, J.G., 1994. Application of experimental results to C–H–O species in natural melts. In: Carroll, M.R., Holloway, J.R. (Eds.), Volatiles in Magmas. Rev. Mineral., vol. 30, pp. 187–230.

Hort, M., 1998. Abrupt change in magma liquidus temperature because of volatile loss or magma mixing: effects on nucleation, crystal growth and thermal history of the magma. J. Petrol. 39 (5), 1063–1076.

Jeffries, T.E., Jackson, S.E., Longerich, H.P., 1998. Application of a frequency quintupled Nd: YAG source (l=213 nm) for laser ablation inductively coupled plasma mass spectrometric analysis of minerals. J. Anal. At. Spectrom. 13, 935–940.

Johnson, M.C., Anderson, A.T., Rutherford, M.J., 1994. Pre-eruptive volatile contents of magmas. In: Carroll, M.R., Holloway, J.R. (Eds.), Volatiles in Magmas. Rev. Mineral., vol. 30, pp. 281–330.

Klerkx, J., 1968. Etude geologique et petrologique de la Valle del Bove (Etna). Ph.D. thesis, Universitè del Liege.

Lange, R.A., 1994. The effect of H_2O, CO_2 and F on the density and viscosity of silicate melts. In: Carroll, M.R., Holloway, J.R. (Eds.), Volatiles in Magmas. Rev. Mineral., vol. 30, pp. 331–369.

Lanzafame, G., Neri, M., Acocella, V., Billi, A., Funiciello, R., Giordano, G., 2003. Structural features of the July–August 2001 Mount Etna eruption evidence for a complex magma supply system. J. Geol. Soc. (Lond.) 160, 531–544.

Lautze, N.C., Harris, A.J.L., Bailey, J.E., Ripepe, M., Calvari, S., Dehn, J., Rowland, S.K., Jones, K.E., 2004. Pulsed lava effusion at Mount Etna during 2001. J. Volcanol. Geotherm. Res. 137, 231–246.

Leake, B.E., Woolley, A.R., Arps, C.E.S., Birch, W.D., Gilbert, M.C., Grice, J.D., Hawthorne, F.C., Kato, A., Kisch, H.J., Krivovichev, V.G., Lunthout, K., Laird, J., Mandarino, J., Maresch, W.V., Nickel, E.H., Rock, N.M.S., Schumacher, J.C., Smith, D.C., Stephenson, N.C.N., Ungaretti, L., Whittaker, E.J.W., Youzhi, G., 1997. Nomenclature of amphiboles: report of the Subcommittee on Amphiboles of the International Mineralogical Association, Commission on New Minerals and Mineral Names. Can. Mineral. 35, 219–246.

Le Maitre, R., 1989. A classification of igneous rocks and glossary of terms. Recommendations of the IUGS Subcommission on the Systematics of Igneous Rocks. Blackwell, Oxford, pp. 1–133.

Leonard, G.S., Cole, J.W., Nairn, I.A., Self, S., 2002. Basalt triggering of the c. AD 1305 Kaharoa rhyolite eruption, Tarawera Volcanic Complex, New Zealand. J. Volcanol. Geotherm. Res. 115, 461–486.

Linde, A.T., Sacks, I.S., 1998. Triggering of volcanic eruptions. Nature 395 (6705), 888–890.

Lo Giudice, E., Rasà, R., 1986. The role of the NNW structural trend in the recent geodynamic evolution of north-eastern Sicily and its volcanic implications in the Etnean area. J. Geodyn. 25, 309–330.

Monaco, C., Catalano, S., Cocina, O., De Guidi, G., Ferlito, C., Gresta, S., Musumeci, C., Tortorici, L., 2005. Tectonic control on the eruptive dynamics at Mt. Etna Volcano (Sicily) during the 2001 and 2002–2003 eruptions. J. Volcanol. Geotherm. Res. 144, 211–233.

Morimoto, N., Fabries, J., Ferguson, A.K., Ginzburg, I.V., Ross, M., Seifert, F.A., Zussman, J., Aoki, K., Gottardi, G., 1988. Nomenclature of pyroxenes. Am. Mineral. 73, 1123–1133.

Morrissey, M.M., Chouet, B.A., 1997. A numerical investigation of choked flow dynamics and its application to the triggering mechanism of long-period events at Redoubt Volcano, Alaska. J. Geophys. Res.-Solid Earth 102, 7965–7983.

Murphy, M.D., Sparks, R.S.J., Barclay, J., Carroll, M.R., Lejeune, A.M., Brewer, T.S., Macdonald, R., Black, S., Young, S., 1998. The role of magma mixing in triggering the current eruption at the Soufriere Hills volcano, Montserrat, West Indies. Geophys. Res. Lett. 25 (18), 3433–3436.

Nakagawa, M., Wada, K., Wood, C.P., 2002. Mixed magmas, mush chambers and eruption triggers: evidence from zoned clinopyroxene phenocrysts in Andesitic Scoria from the 1995 eruptions of Ruapehu volcano, New Zealand. J. Petrol. 43 (12), 2279–2303.

Patanè, D., Chiarabba, C., Cocina, O., De Gori, P., Moretti, M., Boschi, E., 2002. Tomographic images and 3D earthquake locations of the seismic swarm preceding the 2001 Mt. Etna eruption: evidence for a dyke intrusion. Geophys. Res. Lett. 29 (135), 1–4.

Pearce, J.A., 1982. Trace element characteristics of lavas from destructive plate boundaries. In: Andesites, Thorpe (Ed.), Wiley, pp. 525–548.

Phillips, J.C., Woods, A.W., 2002. Suppression of large-scale magma mixing by melt–volatile separation. Earth Planet. Sci. Lett. 204, 47–60.

Pinkerton, H., Norton, G., 1995. Rheological properties of basaltic lavas at sub-liquidus temperatures: laboratory and field measurements on lavas from Mount Etna. J. Volcanol. Geotherm. Res. 68, 307–323.

Pompilio, M., Trigila, R., Zanon, V., 1998. Melting experiments on Mount Etna lavas: the calibration of an empirical geothermobarometer to estimate the eruptive temperature. Acta Vulcanol. 10, 65–75.

Privitera, E., Alparone, S., D'Amico, S., Gambino, S., Maiolino, V., Spampanato, S., Zuccarello, L., 2001. Seismic evidence of magma intrusion at intermediate depth before the July–August 2001 Mt. Etna (Italy) eruption (Proc. AGU Fall Meeting, EOS Trans). AGU 82 (47), F1328.

Richet, P., Bottinga, Y., 1985. Heat capacity of aluminium-free liquid silicates. Geochim. Cosmochim. Acta 49, 471–486.

Rock, N.M.S., 1990. The International Mineralogical Association (IMA/CNMMN) Pyroxene Nomenclature Scheme: computerization and its consequences. Mineral. Petrol. 43, 99–119.

Romano, R., 1982. Succession of the volcanic activity in the Etnean area. Mem. Soc. Geol. Ital. 23, 28–48.

Romano, R., Sturiale, C., 1982. The historical eruptions of Mt. Etna (volcanological data). Mem. Soc. Geol. Ital. 23, 75–97.

Russel, J.K., 1990. Magma mixing processes: insights and constraints from thermodynamic calculation. In: Nicholls, J., Russel, J.K. (Eds.), Modern Methods of Igneous Petrology: Understanding Magmatic Processes. Rev. Mineral., vol. 24, pp. 153–190.

Rutherford, M.J., Devine, J.D., 2003. Magmatic conditions and magma ascent as indicated by horneblende phase equilibria and reactions in the 1995–2002 Soufriere Hills magma. J. Petrol. 44, 1433–1454.

Scaillet, B., Evans, B.W., 1999. The 15 June 1991 eruption of Mount Pinatubo: I. Phase equilibria and pre-eruption P–T–fO_2–fH_2O conditions of the dacite magma. J. Petrol. 40, 381–411.

Snyder, D., 1997. The mixing and mingling of magmas. Endeavour 21/1, 19–22.

Sun, S.S., 1980. Lead isotopic study of young volcanic rocks from mid-ocean-ridges, ocean island and island arcs. Phil. Trans. R. Soc. A297, 409–445.

Taddeucci, J., Pompilio, M., Scarlato, P., 2002. Monitoring the explosive activity of the July–August 2001 eruption of Mt. Etna (Italy) by ash characterization. Geophys. Res. Lett. 29 (8). doi: 10.1029/2001GL014372.

Taddeucci, J., Pompilio, M., Scarlato, P., 2004. Conduit processes during the July–August 2001 explosive activity of Mount Etna (Italy): inferences from glass chemistry and crystal size distribution of ash particles. J. Volcanol. Geotherm. Res. 137, 33–54.

Tanguy, J.C., Condomines, M., Kieffer, G., 1997. Evolution of Mount Etna magma: constraints on the present feeding system and eruptive mechanism. J. Volcanol. Geotherm. Res. 75, 221–250.

Thornber, C.R., Heliker, C., Sherrod, D.R., Kauahikaua, J.P., Miklius, A., Okubo, P.G., Trusdell, F.A., Budahn, J.R., Ridley, W.I., Mecker, G.P., 2003. Kilauea east rift zone magmatism: an episode 54 perspective. J. Petrol. 44, 1529–1559.

Treuil, M., Joron, J.L., 1975. Utilisation des elements hygromagmatophiles pour la simplification de la modelisation quantitative des processus magmatiques. Exemples de l'Afar et de la Dorsale Medioatlantique. Rend. Soc. Ital. Mineral. Petrol. 31 (1), 125–174.

Venezky, D.Y., Rutherford, M.J., 1997. Pre-eruption conditions and timing of dacite-andesite magma mixing in the 2.2 ka eruption at Mount Rainier. J. Geophys. Res.-Solid Earth 102, 20069–20086.

Wood, B.J., Banno, S., 1973. Garnet–orthopyroxene and orthopyroxene–clinopyroxene relationships in simple and complex systems. Contrib. Mineral. Petrol. 42, 109–124.

Wood, D.A., Joron, J.L., Treuil, M., Norry, M., Tarney, J., 1979. Elemental and Sr isotope variation in basic lavas from Iceland and surrounding ocean floor. Contrib. Mineral. Petrol. 70, 319–347.

Woods, A.W., Cardoso, S.S.S., 1997. Triggering basaltic volcanic eruptions by bubble–melt separation. Nature 385 (6616), 518–520.